*Environ. Sci. Technol.* **2007**, *41,* 2485−2490

# Initial Test Results for a Passive Surface Water Fluxmeter to Measure Cumulative Water and Solute Mass Fluxes

HARALD KLAMMLER,[†,‡] MARK A. NEWMAN,[†] ESZTER SZILÁGYI,[†] JULIE C. PADOWSKI,[§] KIRK HATFIELD,*[,†] JAMES W. JAWITZ,[§] AND MICHAEL D. ANNABLE[∥]

*Department of Civil and Coastal Engineering, University of Florida, Gainesville, Florida 32611, Research Center for Geophysical and Geological Studies, Federal University of Bahia, Salvador, Brazil, Soil and Water Science Department, University of Florida, Gainesville, Florida 32611, and Department of Environmental Engineering Sciences, University of Florida, Gainesville, Florida 32611*

The theoretical concept and initial test results of a Passive Surface Water Fluxmeter (PSFM) to directly and simultaneously measure cumulative water and solute mass fluxes in surface water flow systems are presented. The PSFM consists of a symmetric hydrofoil that is vertically installed in a stream and one or more sorbent columns that are connected to the nonuniform flow field around the hydrofoil. Depending on the ambient flow velocity, a flow occurs through each column, which elutes portions of initially present "resident" tracers in the column, while, at the same time, solutes in the water (e.g., contaminants or nutrients) are retained in the sorbent column. Quantification of the resident tracer mass remaining and the mass of solutes sorbed in the column enables determination of the local cumulative or time-averaged water and solute mass fluxes. Laboratory flume experiments show good agreement with independent measurements ($R^2 \geq 0.96$) for instantaneous water fluxes (tested range: 0.3−0.7 m/s), cumulative water fluxes (50−600 L/cm$^2$), and cumulative nitrate fluxes (0.4−5.1 g/cm$^2$). Future work is required to validate the PSFM performance under a larger range of flow velocities, transient flow, and transport conditions and for different hydrofoil shapes.

## Introduction

The assessment of water pollution and, in particular, the measurement of water and solute (e.g., contaminant or nutrient) mass discharges in streams is a fundamental hydrological task for ecological and economical decision making. Flux- and discharge-based data (e.g., nutrient loads) are increasingly being viewed by scientists and law makers as critical information needed to address various components such as source prioritization, risk prediction, compliance monitoring, remediation endpoint evaluation, and contaminant attenuation assessment. Current methods for determining solute discharge often require significant amounts of time and resources to properly sample and process water quality data, making it impractical to monitor every stream or river. Such limitations have impaired the ability of state and federal natural resource management agencies to adequately protect water resources, despite long-standing regulatory protection for surface waters (*1*). Thus, we have the motivation for the development of a passive technology capable of directly and simultaneously measuring cumulative water and solute mass fluxes at various locations in a stream transect.

Numerous methods exist to directly measure water discharge, including tracer dilution (instantaneous or constant injection), acoustic or electromagnetic methods, and methods based on the deployment of hydraulic devices (e.g., weirs or notches). Furthermore, water discharge can be measured indirectly through monitoring the stage of a stream and inferring the discharge from a known stage−discharge relationship. Yet another group of methods is based on the measurement of local flow velocities, e.g., using current meters, within a stream transect, which are then used to calculate the water discharge by applying some standard method (e.g., two-point method, integrated measurement method, etc.). Descriptions of all these methods are widely available in the hydrology literature (e.g., *2*). Measurements of solute concentrations are classically performed by collecting water samples at discrete moments in time and point locations in a stream transect (e.g., *3*). More recently, refs *4* and *5* present passive devices for time-integrated water sampling using submerged bottles that intake water through a permeable material or a capillary hole, respectively. Guidelines for the collection of discharge and water quality data as well as a discussion of sampling strategies at the small watershed scale are provided in refs *6* and *7*, while a comparison between manual and automated sampling is given in ref *8*. Water quality samples are analyzed for their solute concentration, and the local solute mass fluxes are then calculated as the product of the solute concentrations and the water fluxes, which subsequently can be integrated over a transect to obtain solute mass discharge. Spatial variability of solute concentrations and fluxes complicate this process and a respective comparison of surface-grab and cross-sectionally integrated water quality sampling methods is performed by ref *9*.

From the nature of these methods it can be observed that water discharge measurements are basically of instantaneous nature and that cumulative or time-averaged discharges have to be obtained from interpolating and integrating recorded time series data. Furthermore, no method is known that is capable of monitoring solute mass fluxes in either a direct (i.e., without concentration sampling) or timely continuous manner. Hence, the assessment of cumulative or time-averaged water and solute mass fluxes and discharges can be performed with current methods, yet the technical requirements in the field for data acquisition are considerable and involve additional computations to arrive at the final estimates. This is particularly true for solute mass fluxes or discharges and, as a consequence, respective estimates are subject to significant uncertainties due to propagated errors (*10*).

The objective of this manuscript is to show the development of a Passive Surface Water Fluxmeter (PSFM), which is tested in the laboratory under limited flow conditions. The PSFM is capable of directly measuring cumulative or time-

* Corresponding author phone: (352) 392-9537; fax: (352) 392-3394; e-mail: khatf@ce.ufl.edu.

[†] Department of Civil and Coastal Engineering, University of Florida.

[‡] Research Center for Geophysical and Geological Studies, Federal University of Bahia.

[§] Soil and Water Science Department, University of Florida.

[∥] Department of Environmental Engineering Sciences, University of Florida.

10.1021/es061883i CCC: $37.00 
Published on Web 02/24/2007

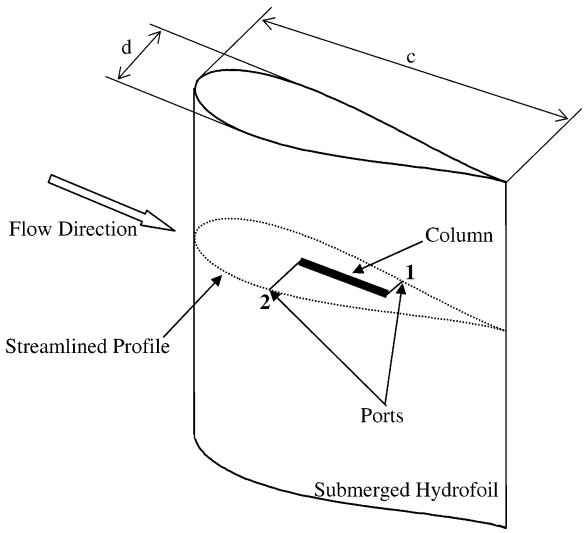


**FIGURE 1. Illustration of a hydrofoil vertically submerged in a stream and aligned to flow direction. A sorbent column is hydraulically connected to the outside flow field at ports 1 and 2.**

averaged water and solute mass fluxes through passive integration of instantaneous water and solute mass fluxes over time. Furthermore, the measurement of solute mass fluxes is direct in the sense that the product of water flux (velocity) and solute concentration is measured directly, rather than each component by itself.

## Materials and Methods

**Description of the PSFM Approach.** The physical principle on which the PSFM is based is the creation of a difference in the static pressures between two points on the surface of an impermeable body that is submerged in a stream. In theory, an unlimited number of shapes can be adopted for this body; however, in order to achieve a well-defined pressure difference, streamlined body shapes are considered to be favorable, since they avoid the creation of a wake (e.g., *11*). In general, these streamlined shapes can be either two or three-dimensional, and symmetric or asymmetric. Practical considerations of construction, installation, and mathematical model development supported the choice of a symmetric hydrofoil PSFM that is vertically installed over the full depth of a stream, and which may freely align with the direction of flow. As shown in Figure 1, a permeable sorptive column is used with the PSFM shell (of width $d$ [L] and chord length $c$ [L]), which is hydraulically connected to the outside flow field through small openings, or ports, in the PSFM shell.

Asymmetric location of the ports provides for the static pressure difference required to drive water flow through the column. The column initially contains a known amount of one or more "resident" tracers with defined sorption properties, which are gradually eluted from the column as water migrates through. After deployment in a flow field, the mass of resident tracers remaining in the column is compared to the initial mass of tracers, and is used to determine the flow through the column. This relative mass remaining, combined with the known hydraulic properties of the column material, enables determination of the hydraulic gradient across the column and thus the static pressure difference between the ports. This pressure difference, in combination with the known qualitative properties of the flow field around the PSFM, is then used to determine the local flow velocities at the ports as well as the velocity of the undisturbed ambient flow.

As the resident tracers are eluted from the column, solutes in the water are simultaneously retained in the column if an appropriate sorbent is provided. The mass of a solute retained in the column during a measurement allows for the estimation of a cumulative solute mass flux. Thus, the working principle of the sorptive column in the PSFM is recognized to be closely related to another type of Passive Fluxmeter, which is installed in monitoring wells to measure cumulative water and solute mass fluxes in porous aquifers (*12*, *13*). By deploying a number of PSFMs with ports and sorbent columns at different depths along a transect of a river, for example, a series of depth profiles may be obtained resulting in a two-dimensional sampling pattern of local cumulative water and solute mass fluxes. This matrix of point measurements can be used to estimate the total water discharge or solute mass load during an observation period.

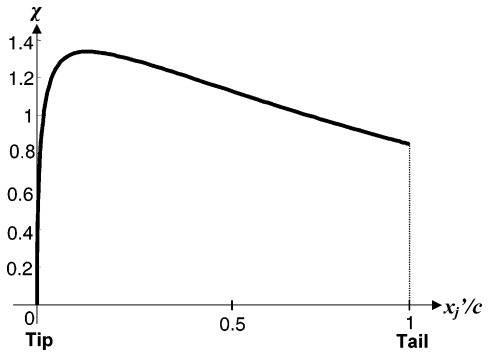


**FIGURE 2. $\chi$-Values for a Joukowsky profile of $b = 0.85$ as a function of normalized position $x_j'/c$ [−] along the longitudinal profile axis. Note that $x_j' = x_j + c - 2ab$ is introduced to locate the tip of the profile at the origin and that the $\chi$-values can be viewed as the normalized velocity distribution for $v_0 = 1$.**

In the present work and as depicted in Figure 1, a symmetric Joukowsky profile (e.g., *14*−*17*) is selected to constitute the cross section of the PSFM hydrofoil. Mathematical expressions of the hydrofoil shape and the properties of the flow field around it are derived in the Supporting Information. The hydraulic model is based on the common assumption of velocity potential flow, which assumes the presence of a sufficiently thin boundary layer on the surface of the profile that does not separate (*11*, *15*). The shape of a Joukowsky profile can be described in a parametric form as follows:

$$x_j = a[\cos\alpha_c - (1-b)]\left[1 + \frac{b^2}{1 - 2(1-b)\cos\alpha_c + (1-b)^2}\right] \quad (1)$$

$$y_j = a\sin\alpha_c\left[1 - \frac{b^2}{1 - 2(1-b)\cos\alpha_c + (1-b)^2}\right] \quad (2)$$

where $x_j$ [L] and $y_j$ [L] are Cartesian coordinates according to Figure 2 of the Supporting Information, $a$ [L] is a scaling factor, $b$ [−] is a parameter ranging from 0 to 1 defining the bluntness of the profile, and $\alpha_c$ [−] is a parameter ranging from 0 to $2\pi$. The magnitude $v_j$ [L/T] of the velocity along the profile is obtained to be

$$v_j(\alpha_c) = \frac{|1 - e^{-2i\alpha_c}|}{\left|1 - \frac{b^2}{[e^{i\alpha_c} - (1-b)]^2}\right|} v_0 = \chi(\alpha_c)v_0 \quad (3)$$

where $v_0$ [L/T] is the ambient flow velocity, $\chi(\alpha_c)$ [−] is the proportionality factor between $v_0$ and $v_j$ for a given location described by $\alpha_c$, and $i$ is the imaginary unit. Figure 2 gives an example of a possible distribution of flow velocities along a Joukowsky profile of $b = 0.85$ in terms of $\chi$-values, which according to eq 3 corresponds to a representation of $v_j$ for $v_0 = 1$. In general, the $\chi$-value of a given location on the

profile can be interpreted as the local flow velocity at that location for $v_0 = 1$, independent of the shape of the PSFM profile. The abscissa $x_j'/c$ [−] in Figure 2 is scaled to unity chord-length, where $x_j' = x_j + c - 2ab$ [L] is introduced to locate the tip of the profile at the origin. By letting $\alpha_c$ range from 0 to $\pi$ in eqs 1 and 3 (due to symmetry the range from $\pi$ to $2\pi$ is identical) the graph of Figure 2 is obtained.

As shown in the Supporting Information, $v_0$ can be determined from a measured head difference $\Delta\varphi$ [L] by using Bernoulli's law as

$$v_0 = \sqrt{\frac{2g\Delta\varphi}{\chi_2^2 - \chi_1^2}} \tag{4}$$

where $\Delta\varphi$ is inferred from the relative (with respect to the initial mass) remaining mass $m_{tr,r}$ [−] of a tracer as

$$\Delta\varphi = \frac{L^2\Theta R_{d,tr}(1 - m_{tr,r})}{k_f t_m} = \frac{LA\Theta R_{d,tr}(1 - m_{tr,r})}{K_f t_m} \tag{5}$$

Herein, $g$ [L/T$^2$] is the gravitational constant, $L$ [L] is the column length, $A$ [L$^2$] the column cross sectional area, $\Theta$ [−] the sorbent water content, and $k_f$ [L/T] is the sorbent hydraulic conductivity. $R_{d,tr}$ [−] is the retardation coefficient of a tracer, $t_m$ [T] is the duration of the measurement, and $K_f = k_f A/L$ [L$^2$/T] is used to represent the hydraulic conductance of the sorbent column. $\chi_1$ [−] and $\chi_2$ [−] are factors obtained from eq 3 corresponding to the respective parameters $\alpha_c$ of the ports on the PSFM profile, which are determined from the position $x_j$ (or $y_j$) of the ports and by inversion of eq 1 (or 2). Since this inversion is not straightforward, Figure 2 can be used to find $\chi_1$ and $\chi_2$ graphically for a Joukowsky profile of $b = 0.85$ given $x_j'/c$.

The solute mass flux $J_{sol}$ [M/(TL$^2$)] is determined from the mass $m_{sol}$ [M] of a solute detected in a column as

$$J_{sol} = \frac{2gLm_{sol}}{Av_0k_f t_m(\chi_2^2 - \chi_1^2)} \tag{6}$$

Equations 5 and 6 assume instantaneous, reversible, and linear tracer and solute partitioning in the sorbent column; however, this assumption can be relaxed by applying a method proposed in ref *12* that is capable of accounting for nonlinear and/or nonequilibrium sorption. Equations 5 and 6 also neglect diffusive and dispersive tracer and solute transport inside the sorbent column with respect to advective transport. While diffusive and dispersive transport does occur inside the sorbent column, ref *12* demonstrated that Peclet numbers for comparable columns and flow velocities indicate advection-dominated transport. Moreover, eq 6 is only valid as long as no solute has left the sorbent column through the down-gradient extreme; otherwise, an equation given in the Supporting Information (page S8) can be applied (which is then only approximate for variable solute concentrations). Note that in contrast to eqs 1, 2, and 3, which are only valid for Joukowsky profiles in theoretically infinite flow domains, eqs 4, 5, and 6 are independently valid of the actual hydrofoil shape and boundary conditions as long as the $\chi$-values of the ports can be determined.

**Physical Design of the PSFM.** While eqs 1 and 2 define the exact shape of a Joukowsky profile to be used as the PSFM cross section in the present work, the required parameters $a$ and $b$ are determined from the aspect ratio $\sigma = d/c$ [−] of the profile as follows:

$$b = 1 - 0.78\sigma \tag{7}$$

$$a = \frac{(2 - b)c}{4} \tag{8}$$

Equation 7 is valid in the range $0 < \sigma < 0.4$ (see also Supporting Information). According to discussions in refs *11* and *15* and for the flow conditions encountered in practical applications, a $\sigma$ of approximately 0.2 is considered a reasonable compromise between a sufficient disturbance of the flow field and the requirement to maintain potential flow everywhere around the PSFM (no wake). For lower expected flow velocities, $\sigma$ can be increased (blunter shapes), while elevated flow velocities may require even smaller values of $\sigma$. Since eq 3 is independent of the scaling parameter $a$ in eqs 1 and 2, an arbitrary scaling of the profile does not affect the velocity distribution around the profile and its absolute size ($c$ and $d$) can be chosen by practical considerations.

As shown in Figure 1 the ports are preferentially located on the down-gradient side of the profile (positive static pressure gradient along the contour when following flow) to reduce the risk of clogging. The ports are furthermore located at opposite sides in order to keep water that leaves the column through port 2 from reentering the column through port 1. While the separation distance between the ports needs to be large enough to provide a sufficient pressure gradient over the sorbent column, the exact locations of the ports can be chosen to facilitate a convenient column handling (see also discussion below). Several resident tracers with different retardation factors may be used in the column to expand the measurement range over orders of magnitude of the cumulative water flux. One tracer may still be available for a reasonable interpretation of the measurement, while others may be either completely or just barely eluted from the column. For each target solute constituent an appropriate sorbent material has to be provided in the column.

**Construction of Hydrofoil.** A 2 mm thick PVC sheet was used to construct a 65 cm tall hydrofoil with design parameters $c = 50$ cm and $\sigma = 0.2$ as represented by the dashed line in Figure 3. The ports used for this series of experiments were located vertically 20 cm from the base of the hydrofoil and distributed horizontally with a spacing of 5 cm along the $x_j'$ axis as indicated by the arrows in Figure 3. This resulted in $x_j' = 13/18/23/28/33$ cm and, according to the discussion above, in $\chi$-values of 1.28/1.22/1.16/1.10/1.04 for ports 1 through 5, respectively.

The continuous line in Figure 3 represents the actual (real) shape of the hydrofoil profile as constructed. Deviations with respect to the design profile require a modification of the design $\chi$-values to 1.22/1.22/1.19/1.13/1.03 (obtained from a fine grid finite difference model (*18*)). Moreover, in order to (approximately) account for the fact that the flow domain in the experiments is not infinite but restricted to a 60 cm wide flume, the law of continuity is invoked at each port location. That is, each modified $\chi$-value is multiplied by a factor $60/(60 - w_p)$, where $w_p$ [L] is the width of the PSFM profile in cm at a given port location ($w_p = 8.6/8.5/7.7/6.3/4.6$ cm for ports 1 through 5, respectively). Thus, the resulting $\chi$-values relevant for the given hydrofoil and flume configuration are 1.42/1.42/1.37/1.26/1.12. Note, that as the ratio of flume width to PSFM width increases this latter correction factor tends to unity and becomes insignificant. This will be the case in typical field situations where the distances to lateral boundaries (e.g., shorelines or neighboring PSFM's in a transect) are much larger than the PSFM width.

**Construction and Analysis of Columns.** Two sorptive columns in series (an anion exchange column and an activated carbon column) were deployed between different ports of the PSFM for observation of tracer elution and solute sorption. The anion exchange columns were packed with BioRad AG-1 × 8 resin (20 × 50 mesh) and used to measure cumulative nitrate ($NO_3^-$) flux, while the activated carbon columns were prepared in a fashion similar to that of the Passive Fluxmeter (*13*). In brief, they were packed with silver-impregnated granular activated carbon (989 20 × 50 mesh:

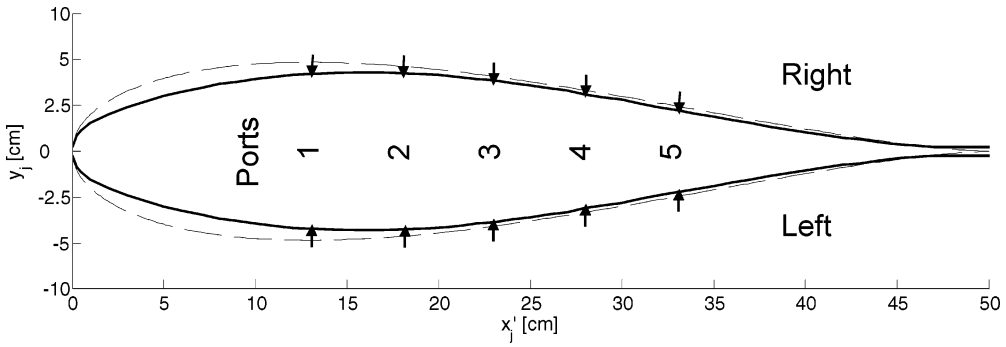


**FIGURE 3. Design (dashed line) and real (continuous line) hydrofoil profiles with port locations (arrows) on both sides.**

Barnebey Sutcliffe Corp., Columbus, OH) prepared with resident tracers ethanol, methanol, isopropyl alcohol, tert-butyl alcohol, and 2,4-dimethyl-3-pentanol for measuring cumulative water flux. Both ion exchange and activated carbon columns were constructed using Pierce 10-mL polypropylene columns (length = 70 mm; diameter = 15 mm). Porous polyethylene discs were used to hold the media in place. The combined hydraulic conductances $K_f$ of the devices (two columns plus tubing to the ports) were determined based upon the observed flowrates through the devices for known head differences. $K_f$ ranged from 0.24 to 0.46 cm$^2$/min for the devices used in the experiments.

Tracer retardation factors were estimated from a column elution experiment following the procedure presented by refs *12* and *13*. For the finer mesh activated carbon (20 × 50 mesh) applied in this study the retardation coefficients $R_d$ were measured as methanol = 6, ethanol = 22, and isopropyl alcohol (IPA) = 119. Nitrate was extracted from anion exchange columns using potassium bromide solution and nitrate analysis was performed colorimetrically using a Bran+Luebbe AutoAnalyzer III (Bran+Luebbe method 696F-82W). Tracers were extracted from the activated carbon columns using isobutyl alcohol (IBA) and tracer analysis was performed using a Perkin-Elmer gas chromatograph with FID detector.

**Flume Experiments.** Laboratory flume experiments were conducted to validate both the hydraulic performance of the PSFM hydrofoil in a flow system as well as the hydraulic and sorptive properties of the sorbent column. The experiments were performed in a recirculating flume (width = 0.6 m; length = 18 m) with a standard Pitot-tube installed upstream of the PSFM and at the depth of the PSFM ports to provide independent flow velocity estimates. Static pressures at both PSFM ports and Pitot-tube were measured using simple tube manometers.

These experiments used the following configurations: (1) Direct (manometer) observations of static head differences between fixed port locations for different flow velocities to evaluate the validity of the assumption of velocity potential flow around the PSFM hydrofoil for the range of flow velocities provided by the flume (0.3−0.7 cm/s; corresponding flow depths: 50−30 cm). A subdivision into experiments (1a) and (1b) refers to measurements between port 1 on the left and port 5 on the right side and port 1 on the right and port 5 on the left side, respectively, in order to confirm symmetry of the flow field. (2) Direct (manometer) observations of static head differences between different port locations for (approximately) equal flow velocities to validate the theoretical distribution of static pressures along the PSFM. The observed head differences in (1) and (2) were used to obtain estimates of $v_0$ from eq 4. (3) Observing tracer elution and solute sorption in a sorbent column at fixed ports for (approximately) equal flow velocities (59−67 cm/s) and solute concentrations (7.80−9.27 mg/L) but different measurement periods (15−147 min). Detected relative remaining tracer masses in the sorbent column were used in eqs 4 and 5 to estimate time averages of $v_0$ and to subsequently obtain the cumulative water fluxes ($v_0 t_m$). Furthermore, solute masses detected in the sorbent column were used in eq 6 to estimate time averages of $J_{sol}$ and to subsequently obtain the cumulative solute mass fluxes ($J_{sol} t_m$). In this experiment the sorbent columns were kept outside the PSFM and the flume, and an air bubble was injected into the tubing in order to visualize flow between the ports.

## Results and Discussion

**Flume Test Results.** Flow velocity data obtained from experiments (1) and (2) are plotted in Figure 4 against independent measurements using a Pitot-tube (considered as "true" values). The zero intercept regression line is fitted to the combined set of data points from experiment (1) and indicates very good agreement between the PSFM and Pitot-tube estimates of flow velocities within the tested range. No consistent asymmetry can be identified between experiments (1a) and (1b). Both the first and last data points of experiment (1) are associated with error bars corresponding to a ±0.5 mm interval on measured head differences for the Pitot-tube and ±1 mm interval on measured head differences between PSFM ports. These intervals are due to fluctuations in observed pressure heads related to a locally unsteady water surface in the flume, which occurs to a stronger degree around the PSFM. The degree of this uncertainty decreases gradually as the flow velocity increases and uncertainty intervals for intermediate flow velocities can be approximately interpolated from the error bars shown. The results of experiment (2) in Figure 4 are obtained from pairing up port 5 on the right side with, respectively, ports 1, 2, 3, and 4 on the left side. Four measurements were taken for each of the four port combinations at approximately the same flow velocity. The resulting 16 (partially identical) data points again indicate a good agreement with Pitot-tube flow velocities, which is reflected by a mean error of 3.6 cm/s (approximately 5%) with a standard deviation of 2.0 cm/s and no significant tendency of errors between port pairs. However, in theory, uncertainties in manometer readings propagate much stronger into the final result for measurements between closer ports where expected head differences are smaller (error bars not shown; see discussion under "Sensitivity Analysis" below).

Figure 5 represents the results obtained from experiment (3). Figure 5a depicts measured cumulative water fluxes over a range of approximately 50−600 L/cm$^2$ against respective true values calculated from Pitot-tube velocity measurements. Figure 5b depicts measured cumulative nitrate fluxes over a range of 0.4−5.1 g/cm$^2$ against respective true values obtained from Pitot-tube velocity measurements and solute concentration sampling of the flume water. The zero intercept regression lines show a very good agreement between estimated and true fluxes over approximately an order of magnitude range in each case.

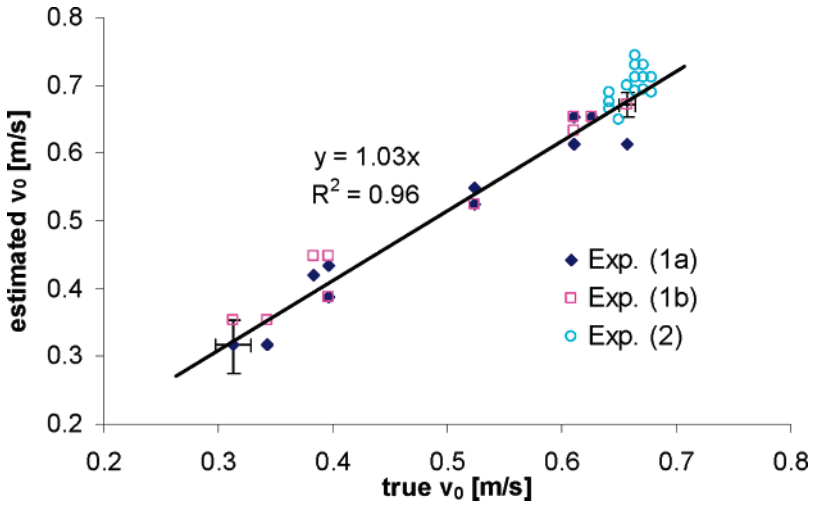


**FIGURE 4. Estimated flow velocities from PSFM against true values (Pitot-tube) for different flow velocities and port combinations: experiment (1a), port 1 left with port 5 right; exp. (1b), port 1 right with port 5 left; exp. (2), port 5 right with ports 1, 2, 3, 4 left (4 measurements with each port pair). Static head differences between ports were obtained from manometer readings with error bars indicating approximate uncertainty intervals for expreriments 1a and 1b due to manometer readings. Error bars for intermediate flow velocities can be approximately interpolated from error bars shown. Regression line forced to zero intercept.**

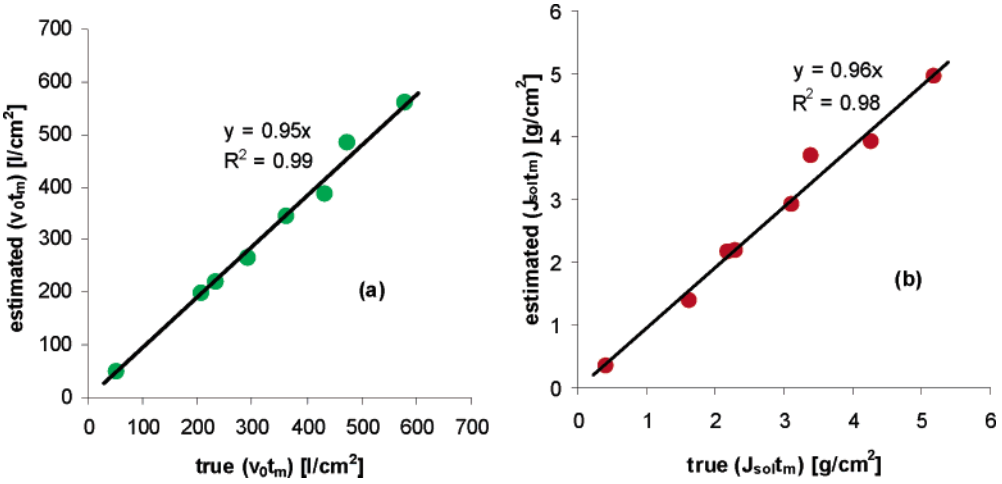


**FIGURE 5. Estimated and true cumulative water (a) and solute mass (b) fluxes. Estimated values were obtained from detected tracer and nitrate masses in the sorbent column, while true values were obtained from Pitot-tube measurements and nitrate concentration sampling in flume water. Regression lines forced to zero intercept.**

**Sensitivity Analysis.** The parameters involved in the estimation of water and solute mass fluxes and their respective impacts on the final estimates can be identified from eqs 4 through 6. Equation 4 shows that relative errors in $\Delta\varphi$ propagate less than proportional (by the square root) to the estimate of $v_0$. For example, a 10% error in $\Delta\varphi$ would translate into a 5% error in $v_0$. By expanding the denominator into a product it can be furthermore observed that errors in the $\chi$-values propagate into $v_0$ to the power $-1/2$ with both the sum and difference between $\chi_1$ and $\chi_2$. In addition, it is desirable in the design of the PSFM to position the ports such that the local flow velocities at their locations are sufficiently different (e.g., ports 1 and 5). This avoids the generation of large absolute errors in $v_0$ due to errors in $\Delta\varphi$ and a large factor $1/(\chi_2^2-\chi_1^2)$. In an analogous manner, eq 5 permits quantification of the impact of errors in the remaining parameters on $\Delta\varphi$ and subsequently $v_0$. It is worthwhile to note that relative errors in $m_{tr,r}$ that may result from tracer mass extraction and quantification propagate proportionally into $\Delta\varphi$ and, hence, to the power $1/2$ into $v_o$. Inspection of eq 6 reveals that relative errors in $m_{sol}$ propagate proportionally into the estimate of $J_{sol}$, while after substitution of eqs 4 and 5 in 6 the role of the $\chi$-values can be seen to remain identical to what is discussed above for the $v_0$ estimate. Relative errors in $m_{tr,r}$ manifest to the power $-1/2$; a more detailed discussion on the impact of errors in $m_{tr,r}$ on the $v_0$ and $J$ estimates, which is also applicable here, is presented by ref *12*, who define an optimum range of approximately $0.3 < m_{tr,r} < 0.7$ for error minimization.

While the quadratic relationship between $\Delta\varphi$ and $v_0$ introduced by Bernoulli's law has a favorable effect on the propagation of relative errors (less than proportional), the application of eq 4 leads to an estimate of $v_0$ that is equivalent to the quadratic mean of a timely variant flow velocity $v_0(t)$ under transient conditions. However, as shown in the Supporting Information, for a decreasing coefficient of variation in $v_0(t)$, the estimate of eq 4 approaches the desired arithmetic mean of $v_0(t)$. As further shown in the Supporting Information, the estimate of $J_{sol}$ of eq 6 approaches the arithmetic mean as the coefficients of variation in both $v_0(t)$ and solute concentration decrease or, for significant variability in the solute concentration, as the correlation between them decreases. It is left for future work to quantify the explicit conditions for the validity of eqs 4 and 6 in terms of arithmetic mean estimates under transient flow conditions and to validate respective results experimentally. However, using

Manning's equation for flow in open channels and the $^1/_7$ power law for flow velocity variations over flow depth it can be demonstrated (see Supporting Information) that $v_0$ at a constant elevation above a channel bottom is only proportional to the $^1/_3$ power of the channel discharge (e.g., a 100% increase in discharge only causes a 26% increase in $v_0$), which acts in favor of limiting the variability in $v_0(t)$.

**Limitations and Future Work.** The presented initial test results are encouraging as to the potential of the PSFM method to measure cumulative water and solute mass fluxes in natural or artificial open surface water flow systems. And like other recent developments in environmental monitoring (*19*), future studies are required at both the laboratory and field level to investigate a number of yet unanswered questions. For example, what can we expect in terms of performance under transient flow and transport conditions, or the potential to measure depth profiles of $v_0$ and $J_{sol}$ using sorbent columns at different depths with a single PSFM hydrofoil. In addition, more extensive test series are required to enlarge the range of flow velocities below 0.3 and above 0.7 m/s. In this context, the performance of different PSFM profile shapes can be investigated for different expected flow velocity ranges. For example, blunter profiles (closer to circular) could prove advantageous for lower flow velocities to ensure sufficiently large head differences between ports, while the low flow velocity does not yet provoke a wake downstream of the device. Conversely, more slender profiles may be required for higher flow velocity ranges in order to avoid the disturbance of velocity potential flow around the hydrofoil by downstream wakes. In fact, the family of Joukowsky profiles proposed here possesses two limiting cases that are particularly appealing due to their simple construction: (1) a circular cross section ($b = 0$ in eqs 1 and 2) resulting in a cylindrical PSFM (tube) and (2) a cross section that has collapsed to a line ($b = 1$ in eqs 1 and 2), which resembles the case of a Pitot-tube. Possibilities exist to achieve a free adjustment of the PSFMs of different cross sections to variable flow directions; however, issues of cinematic stability (lateral vibrations of PSFM tail) were observed in the present experiments whenever the hydrofoil was left to freely rotate in the flume and need to be addressed in the future.

In addition, focusing on field applications, the question of possible clogging of the ports needs to be investigated. Ports on the upstream side of the PSFM are considered more likely to become clogged by solids (e.g., Pitot-tube). Studies are needed to evaluate if the current port locations on the downstream side of the hydrofoil can avoid clogging effectively; also, different materials (currently PVC) for the PSFM shell may be tested and ways to install the sorbent columns inside the hydrofoil investigated. Furthermore, possible complications may occur in situations where water level fluctuations can temporarily leave ports above the water surface and the effects of naturally occurring flow nonuniformities at the scale of the PSFM size need to be investigated. Bacterial growth inside the sorbent column can undermine the interpretation of remaining tracer masses in terms of flow velocities and sorbent materials need to be found for a range of potential target solutes. Alternatively, the deployment of active probes to measure flow rates and solute concentrations between PSFM ports can be investigated. Finally, questions about cross-sectional integration of multiple flux measurements with associated uncertainty estimates need to be answered and PSFM end user costs compared to traditional methods.

## Acknowledgments

This research was partially funded under a NASA Glenn Research Center Grant (NAG3-2930), by the United States Department of Agriculture National Research Initiative (award 2003-35102-12868), and the Florida Water Resources Research Center under a grant from the U S. Department of Interior (06HQGR0079). We gratefully acknowledge the support of the HTBLA-Weiz, Austria, for constructing the PSFM hydrofoil.

## Supporting Information Available

More details about flow field calculations and PSFM shape design as well as the derivation of the formulas for estimation of water and solute mass flux; calculations for sensitivity analysis under transient flow and transport conditions. This material is available free of charge via the Internet at http://pubs.acs.org.

## Literature Cited

(1) Cooter, W. S. Clean Water Act assessment processes in relation to changing US Environmental Protection Agency management strategies. *Environ. Sci. Technol.* **2004**, *38* (20), 5265−5273.
(2) Gupta, R. S. *Hydrology and Hydraulic Systems*, 2nd ed.; Waveland Press: Long Grove, IL, 2001.
(3) Rock, L.; Mayer, B. Tracing nitrates and sulphates in river basins using isotope techniques. *Water Sci. Technol.* **2006**, *53* (10), 209−217.
(4) Panno, S. V.; Krapac, I. G.; Keefer, D. A. A New Device for Collecting Time-Integrated Water Samples from Springs and Surface Water. *Environ. Eng. Geosci.* **1998**, *4* (3), 375−383.
(5) Selker, J. S.; Rupp, D. E. An environmentally driven time-integrating water sampler. *Water Resour. Res.* **2005**, 41, W09201, doi:10.1029/2005WR004040.
(6) Harmel, R. D.; King, K. W.; Slade, R. M. Automated storm water sampling on small watersheds. *Appl. Eng. Agric.* **2003**, *19* (6), 667−674.
(7) Harmel, R. D.; King, K. W.; Haggard, B. E.; Wren, D. G.; Sheridan, J. M. Practical guidance for discharge and water quality data collection on small watersheds. *Trans. ASABE* **2006**, *49* (4), 937−948.
(8) Ging, P. *Water-Quality Assessment of South-Central Texas: Comparison of Water Quality in Surface-Water Samples Collected Manually and by Automated Samplers*; USGS Fact Sheet FS-172-99; U.S. Geological Survey: Washington, DC, 1999.
(9) Martin, G. R.; Smoot, J. L.; White, K. D. A comparison of surface-grab and cross-sectionally integrated streamwater-quality sampling methods. *Water Environ. Res.* **1992**, *64* (7), 866−876.
(10) Harmel, R. D.; Cooper, R. J.; Slade, R. M.; Haney, R. L.; Arnold, J. G. Cumulative uncertainty in measured streamflow and water quality for small watersheds. *Trans. ASABE* **2006**, *49* (3), 689−701.
(11) Gerhart, P. M.; Gross, R. J.; Hochstein, J. I. *Fundamentals of Fluid Mechanics*, 2nd ed.; Addison-Wesley Publishing Company: New York, 1992.
(12) Hatfield, K.; Annable, M. D.; Cho, J.; Rao, P. S. C.; Klammler, H. A direct method for measuring water and contaminant fluxes in porous media. *J. Contam. Hydrol.* **2004**, *75*, 155−181.
(13) Annable, M. D.; Hatfield, K.; Cho, J.; Klammler, H.; Parker, B.; Cherry, J.; Rao, P. S. C. Field-scale evaluation of the passive flux meter for simultaneous measurement of groundwater and contaminant fluxes. *Environ. Sci. Technol.* **2005**, *39* (18), 7194−7201.
(14) Prandtl, L.; Tietjens, O. G. *Fundamentals of Hydro- and Aeromechanics;* Dover Publications: New York, 1934.
(15) Prandtl, L.; Tietjens, O. G. *Applied Hydro- and Aeromechanics;* Dover Publications: New York, 1934.
(16) Milne-Thomson, L. M. *Theoretical Hydrodynamics*, 2nd ed.; The Macmillan Company: New York, 1950.
(17) Betz, A. *Konforme Abbildung; Zweite Auflage;* Springer-Verlag: Berlin, 1964.
(18) Harbaugh, A. W.; McDonald, M. G. *Programmer's Documentation for MODFLOW-96, an Update to the U.S. Geological Survey Modular Finite-Difference Ground-Water Flow Model*; USGS Open-File Report 96-486; U.S. Geological Survey: Washington, DC, 1996.
(19) Campbell, T. J.; Hatfield, K.; Klammler, H.; Annable, M. D.; Rao, P. S. C. Magnitude and directional measures of water and Cr(VI) fluxes by passive flux meter. *Environ. Sci. Technol.* **2006**, *40* (20), 6392−6397.

*Received for review August 6, 2006. Revised manuscript received December 15, 2006. Accepted January 22, 2007.*

ES061883I